Received: 8 March 2021 | Revised: 24 June 2021 | Accepted: 26 July 2021

DOI: 10.1002/sat.1423

SPECIAL ISSUE PAPER

WILEY

Design of a 3D ray-tracing model based on digital elevation model for comprehension of large- and small-scale propagation phenomena over the Martian surface

Stefano Bonafini | **Claudio Sacchi**

Department of Information Engineering and Computer Science, University of Trento, Trento, Italy

Correspondence
Stefano Bonafini, Department of Information Engineering and Computer Science, University of Trento, Povo, Trento 38123, Italy.
Email: stefano.bonafini@unitn.it

Summary

The aim of the scientific community, towards the investigation of solutions able to favor a futuristic human settlement on Mars, also concerns ad hoc communication systems and wireless networks to be deployed over the "Red planet." However, the state-of-the-art appears to be missing of realistic and replicable models for understanding the radio propagation over precise Martian locations. This means that performing solid simulations, rather than roughly approximated ones, is really a tough task. Thus, this paper describes the design of a 3D ray-tracing simulator based on high-resolution digital elevation models (DEMs) for the evaluation of Martian large-scale and small-scale phenomena in the S and EHF bands. First, by taking advantage of the Cole–Cole equations, we computed the complex permittivity of the JSC Mars-1 Martian regolith simulant. Then, we developed a 3D tile-based structure of the Gale crater, thanks to its DEM, and finally, we implemented a ray-tracing algorithm for outdoor environments able to trace the line of sight (LOS), the first and second reflections of a radio frequency (RF) signal between a transmitter (TX) and a receiver (RX) over the 3D structure. The results focus on estimating path losses, shadowing values, outage probability, and on the parametrization of multipath channels for selected areas and subareas, presenting heavily different morphological features, of the Gale crater. Moreover, some brief considerations about dust storms and atmosphere harmful effects on propagation will be drawn.

KEYWORDS
digital elevation model, Gale crater, large-scale phenomena, Martian surface, radio propagation, ray tracing, small-scale phenomena

Abbreviations: DEM, digital elevation model; GA1 and GA2, "Gale Crater—Area 1" and "Gale Crater—Area 2"; LOS, line of sight; RF, radio frequency; RX, receiver; SA, subarea; TX, transmitter.

Stefano Bonafini and Claudio Sacchi are equally contributing authors.

1 | INTRODUCTION

At the time we are writing this article, the landing of the "Mars Perseverance rover" on the so-called "Red planet" is only a couple of days away. As the general excitation about this event increases, we are here hoping that it will all turn out for the best. Indeed, this will be a milestone in the history of deep space missions, which, hopefully, will take the first flying object, that is, the "Mars Helicopter Scout" or "Ingenuity," over another world.[1] Besides its absolute importance due to the first lift-off from the Martian surface and the subsequent autonomous flight, we should highlight its relevance alleging that, in the next few years, Mars will be populated by intelligent machines in the form of landers, rovers, and even drones, as in this case. For this reason and with the idea of favoring the human settlement, which, as reported in Foust,[2] will only be feasible in 2037 "without accepting large technology development, schedule delay, cost overrun, and budget shortfall risks,"[3] lately, researchers proposed wireless network architectures for mobile communications based on the devices already deployed over the Martian environment. For example, in Sacchi and Bonafini,[4] it is described a network architecture for local wireless communications based on landers, treated as eNodeB, that is, the base station (BS), of the cellular network, and rovers, which basically are the user equipment (UE). The idea, which was enhanced in Bonafini and Sacchi[5] by showing the potentiality of a turbo coded hybrid-LTE embryo, aims at increasing the ability of in situ post processing of gathered data along with providing wideband and robust communication links. Moreover, the authors claim that the "LTE on Mars" infrastructure will also serve the astronauts, that will land on the "Red planet," for the communications, in a first instance, between them and, secondary, to the Earth.

Thus, as far as we consider supporting a future and futuristic astronauts crew on Mars through short- and long-range high data rates communications—embarking also a sociality aspect—it appears to be of crucial relevance the analysis of communication systems, and extending the network infrastructure, that the scientific community, and in particular telecommunications engineers, will have to pursue in order to understand the advantages, limits, and drawbacks of the selected technology to be used on Mars. And to do that, it is needed to perform solid simulations based on the correct modeling of the environment we are taking into account. However, in Sacchi and Bonafini[4,5] as well as in other pieces of research that later will be discussed, the results appears to be preliminary due to the lack of a model able to realistically evaluate the radio frequency (RF) propagation over Mars terrains, that is, the knowledge about Martian large-scale and small-scale phenomena.

Generally, software simulations are done to measure the performance of communication systems in terms of quality of service (QoS), reliability, and resilience metrics. Most of the commercial software, despite being different in their structures and workflows, are parameterized, in order to simulate a wireless environment, by characterizing the channel through path losses, shadowing values and path delays and gains for the multipath propagation. On Earth, such variables are easily measured by installing transceivers on urban, suburban, rural, or mountainous areas and testing the RF propagation, thus gathering samples at the receiver side, from which we obtain the received power and delays of arrivals. Recently, these on-field tests were partially substituted by exploiting the ray-tracing algorithm, as done in Fuschini et al[6] for outdoor environment or in Hosseinzadeh et al[7] for indoor situations, which uses as input a 3D representation of the area we want to study. However, when dealing with the Martian surface, on-field tests are not, at least for our epoch, feasible—although it is possible to do approximated tests on Martian analog on Earth or reproducing a similar Martian environment as done by the Rover Operation Control Center in Turin[8]—and, as far as we know, the literature does not propose solutions to properly simulate the RF transmission over the surface of the "Red planet" along with in-depth analysis of the impairments affecting the propagation.

This paper will present, by enhancing the work started in Bonafini and Sacchi,[9,10] the design of a ray tracing-based simulator, which estimates the line of sight (LOS), first reflections, and second reflections of an RF signal generated by the morphology of the Gale crater, represented through a high-resolution digital elevation model (DEM) puts as input to the MATLAB's implementation. NASA provided a high-resolution DEM of the Gale crater—1 m/px, which is assumed it was probably a salty iced lake in some Martian epochs.[11] Thus, this is a particularly relevant area to be studied. The model, that we designed, estimates through the Cole–Cole equations the electrical properties of a possible Martian replicant soil, that is, JSC Mars-1, in order to compute the amount of power lost/reflected into/from the medium, that is, large rocks and cliffs. The DEM is modeled in MATLAB by implementing a 3D structure composed of tiles, whose side length is equal to the DEM's resolution. The closest vertices of the tiles are connected in order to build the walls of the structure. The paper will continue by studying the samples gathered from multiple simulations in terms of large-scale phenomena, that is, path loss and shadowing, and small-scale phenomena, that is, multipath propagation. Few considerations will be done about the outage probability and other kind of large-scale attenuation, such as dust storms and atmosphere attenuation—no less important than the other.

The rest of the paper is structured as follows: Section 2 will present an overview of related work, Section 3 will show the proposed DEM-based ray-tracing methodology for Martian channel modeling, and Section 4 will present and discuss some simulation results. Paper conclusion and hints for future work will be drawn in Section 5.

2 | LITERATURE REVIEW

The literature is quite rich when dealing with the topic of RF propagation on Earth, along with all the analysis on attenuation, which negatively affect the performance of communication systems at the physical (PHY)-layer side. Unfortunately, we cannot say the same for what concerns

wireless communications on Mars. However, there are few pieces of research that has faced the problem. The early works found in the state of the art, which analyze the multipath propagation over some precise Martian locations, such as the Meridiani planum—where the Mars Exploration Rover (MER) "Opportunity" landed to find evidence of liquid water[12] in 2004—and the Gusev crater, which is probably an ancient lake[13]—where the second rover of the MER mission called "Spirit" landed, are the ones in Chukkala and De Leon[14] and Daga et al.[15] Chukkala and De Leon,[14] as well as Daga et al,[15] exploited the ICS telecom, a proprietary software by ATDI.[16] As we know, the environment, in which a communication occurs, sensibly affects the RF transmission; indeed, the objects in the middle of the path between TX and RX, which can move with a certain velocity, create reflections of the signal, thus multiple paths characterized by an intrinsic delay due to the increased distance with respect to the LOS.

This brief explanation almost covers the so-called small-scale phenomena, that is, multipath propagation and Doppler effect, which is a frequency shift due to the motion of the transceiver. Through the Longley–Rice, or also called "Irregular Terrain Model" (ITM), they presented few samples of received power and delay spread of simulated RF transmissions in the S band ($f = 2.4$ (GHz)). They considered DEMs of the two landing sites of the MER missions with a resolution of 11 m/px. The results in Chukkala and De Leon[14] exhibit power delay profiles (PDPs) for various distances in between the transceiver. For a 100-m transmission, the 92% of the computed RMS delay spread values are lower than 0.72 μs with the RMS maximum delay spread around 0.75 μs, which on Earth can be compared to the delay spread experienced on an urban area.[17] As expected, by increasing the distance to 1000 m, the percentage of RMS delay spread values below 0.72 μs decreases to the 72%, while the maximum RMS delay significantly increases to 3.08 μs, which on Earth it could represent a mountainous area. Daga et al[15] concentrate more on the testing of the IEEE 802.11a and b PHY-layer over the MER landing areas. However, they presented also some more results regarding possible Martian PDPs, introducing also the 5-GHz working frequency, by basically exploiting the methodology in Chukkala and De Leon.[14]

It is interesting to see that, besides the fact that most of the times the received power and RMS delay spread values, respectively, decrease and increase with higher distances, some favorable terrain conditions lead to a Fresnel zone clearance, thus to better transmission conditions and higher received power and lower RMS delay spread. Although these are really solid works, they probably lack in the description of the model; indeed, the arrangement used in order to estimate the PDPs is not detailed enough to be replicable. Moreover, the ITM, which is a radio propagation model that makes predictions on the signal attenuation expressed as a function of distance, exhibits shortcomings when dealing with knife-edge obstacles obstructing the propagation.[18] To conclude, the number of samples shown in both works does not allow approximating realistic Martian channels, neither understanding the behavior of the so-called large-scale phenomena.

For what concerns large-scale phenomena, we can individuate terms that steady decrease the power of an RF signal (path loss), due to the distance between TX and RX, which fluctuates around the mean (shadowing) due to reflection and scattering during the transmission. To the best of author's knowledge, in the literature, we can find only a couple of works exposing such a topic for simulation purposes. To be precise in Del Re et al[19] and Pucci et al,[20] where the small-scale phenomena are treated by representing a flat Martian area with a Ricean channel (LOS environment) and a rocky area with a Rayleigh channel (NLOS environment), the path loss is computed by assigning a third-order exponent to the common free-space path loss (FSPL) in order to approximate for highly scatterers terrains. On the other hand, this evaluation is mostly empirical; thus, it is difficult to know if this approximation could fit a Martian area, and if so, which Martian area.

Even the atmosphere negatively impacts on the propagation of the signal by attenuating the received power. This happens mostly in the extremely high-frequency (EHF) band; indeed, at this level, the wavelength of an EHF signal is comparable to the dimension of the molecules and elements composing the atmosphere. The "collision" between these two parties generates scattering and absorption, which are translated into attenuation.[21] As well as the atmosphere, dust storms, which are really frequent on the surface of Mars, and even clouds and fogs can act as attenuators. This is well explained in NASA.[22] As reported, the troposphere, that is, low atmosphere, is the main agent on the degradation of the RF signal. Furthermore, for high frequencies (f > 10 GHz), it should be considered the attenuation due to clouds and fogs, which is not negligible. The last actor to be considered is the attenuation due to dust storms. As commonly known, they are remarkable features of the Martian surface; indeed, they were documented since the beginning of Mars explorations in the 1960s.[23] Most of the spacecrafts and rovers sent to the "Red planet" noticed such an event, which is really frequent in spring and summer. Dust clouds arise from the surface producing walls of sand with a spatial dimension that ranges between few kilometers to more than 2000 km to even more, which creates a global dust storm encircling the whole planet. This can have a strong impact on RF propagation. From NASA,[23] the worst case, fixing a 10-km dust storm, can reduce the received power of 3 dB for a 32-GHz signal.

In the next sections, we will enhance the discussion regarding these kinds of large-scale phenomena by exploiting the information in NASA[22] and obtaining few results for a frequency span among 1 and 100 GHz and a distance between TX and RX ranging in the interval $d = [1, 10{,}000]$ m.

3 | METHODOLOGY

This paper will present in the next paragraph the design of a 3D ray-tracing model for outdoor scenarios taking as input high-resolution DEMs, which photograph the elevation of Martian areas, such as the Gale crater as considered in this work. Along with the in-depth narration about the simulator, we will discuss how to properly analyze the gathered data exiting from the simulator in order to estimate large-scale and small-scale

phenomena occurring on the surface of Mars. This section is divided into Section 3.1, which will detail the simulator, and Section 3.2, which clarifies the workflow.

3.1 | Simulator

Now, we should explain how to implement the core of this activity, that is, the simulator. As already mentioned before, we developed everything in Matlab environment, a commercial software for programming algorithm and creating models.[24] It was chosen among other tools thanks to its solidity, its exorbitant number of usable ad hoc built-in functions, and its large community that continuously helps the improvement of the technology with external packages and integrable scripts. The following subsubsections will follow the steps of our workflow, which will then be resumed in Section 3.2.

3.1.1 | 3D Martian structure from DEM

Few DEMs with a high resolution are available. One of them is, for sure, the "Mars MSL Gale Merged DEM 1m v3" with a resolution of 1 m/px,[25] which is absolutely enough when dealing with transmissions of hundreds of meters.

It is the "elevation" photo of the Gale crater, an area probably formed 3.7 billion years ago from the downfall of a meteor, which was selected to be the landing site of the "Curiosity" rover in 2012. It is mostly characterized by flat areas made of layered sediments and a central peak, as correctly depicted by Kevin Gill in Figure 1. Researchers found that, with any luck, water flowed into the Gale crater from rivers fed by rains and melting snow. Thus, it became a lake as in Figure 1. Its importance is so justified by the probability of discovering signs of the presence of water, therefore, proof of possible lifeforms in some Martian era. However, for the purposes described in our paper, this area has been exploited in order to construct a 3D structure upon which implementing our RF propagation simulator.

We cropped the DEM into two areas, strongly presenting differences in their morphological structure. The first area, which will be called for simplicity "Gale Crater—Area 1" (GA1), is extruded from the center of the DEM. Consequently, its center point is the middle point of the entire DEM. The second area is obtained by dividing the DEM into three equally spaced slices, where the center of the "Gale Crater—Area 2" (GA2) is the intersection between the lowest red dotted line and the vertical one in Figure 2B. The two areas, both with side length of 1000 m, represent, respectively, an almost flat area and a rocky yet steep one, as clearly visible from Figure 3, where the blue squares are the subdivision of the main areas along their diagonals. However, we will return on this when we will discuss the results in Section 4. Now, what is really demanding to point out is how to create the 3D areas in Matlab.

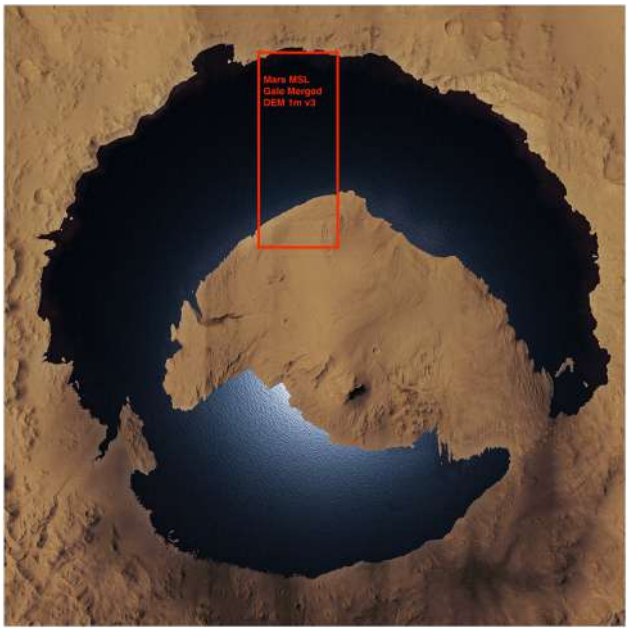

FIGURE 1 Hypothetic lake onto the Gale crater rendered thanks to CTX orthoimagery, digital terrain model data, and Blender with Cycles. Credit: Kevin Gill

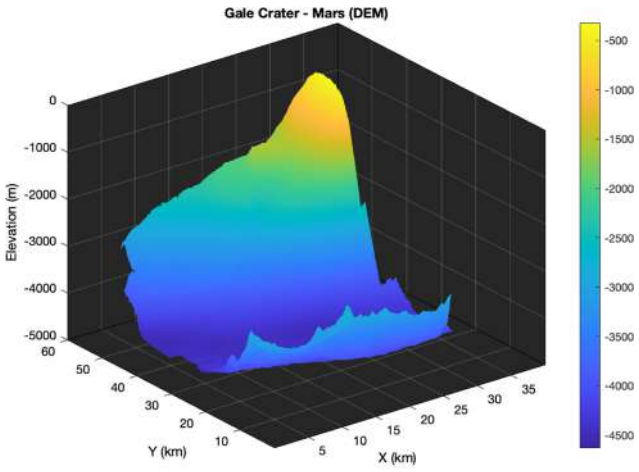

(A)

3D-plot of the Gale Crater DEM

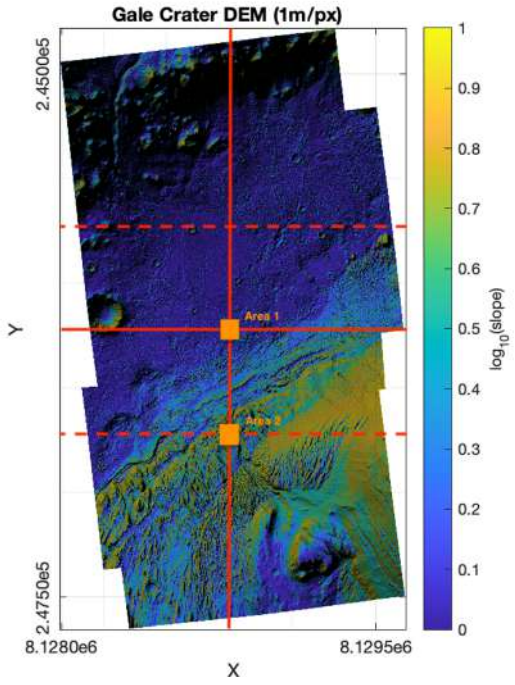

(B)

2D-plot of the Gale Crater DEM

FIGURE 2 (A) 3D plot of the "Mars MSL Gale Merged DEM 1m v3" better highlighting the gradient of the area. (B) 2D plot of the "Mars MSL Gale Merged DEM 1m v3" highlighting the slopes of the central peak, or mountainous area, which raises from the crater. The orange squares depict the cropped areas

A DEM is an array of pixel, whose values are the quote of the area they are representing. Consequently, by defining a set of points $P = [p1, p2, p3, p4]$ in a three-dimensional space, each pixel can be modeled as a tile with side length equal to the DEM's resolution. With $n = [1, 2, \ldots N]$ the nth pixel of the cropped area, the 3D structure is built by interpolating the closest vertices of the nth tile along the z-axis. If we consider pixel n as in Figure 4, the walls between pixel n, $n-1$ and n, $n+1$ are easily obtained, respectively, by connecting $p_1(n)$ and $p_4(n-1)$, $p_2(n)$ and $p_3(n-1)$, $p_3(n)$ and $p_2(n+1)$, and $p_4(n)$ and $p_1(n+1)$. The repetition of this operation along the x-axis and y-axis direction, for the total number of pixel, leads to a floor matrix and a wall matrix, which are both used as input to the 3D ray-tracing algorithm. Thus, the Martian environment is, now, geometrically reproduced by the 3D tile-based structure.

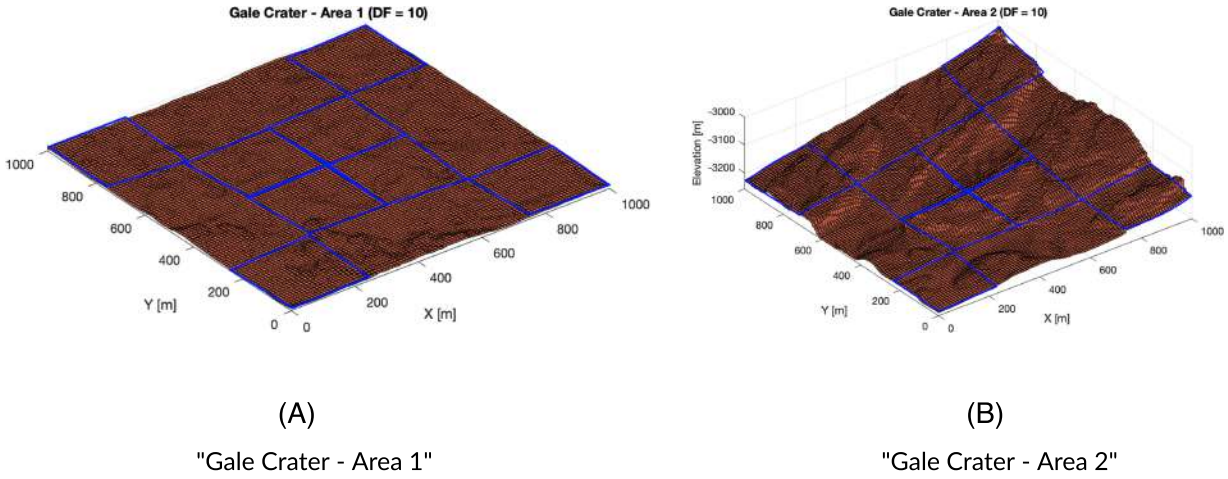

(A) "Gale Crater - Area 1"

(B) "Gale Crater - Area 2"

FIGURE 3 (A) Plot of the 3D tile-based structure of the "Gale Crater—Area 1." In blue the cropped subareas with side length 250 m. (B) Plot of the 3D tile-based structure of the "Gale Crater—Area 2." In blue the cropped subareas with side length 250 m

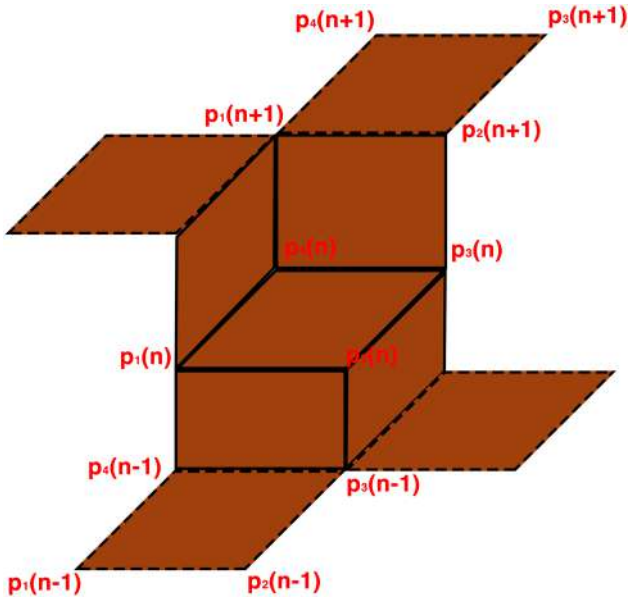

FIGURE 4 Pictorial representation of the interpolation between tiles constructing the 3D structure in Matlab

3.1.2 | Complex permittivity of Martian soil

The geometrical representation of the area is necessary when we estimate the reflections of the RF signal propagated over the structure. However, it is not enough to characterize the Martian environment. Indeed, as commonly known, the electrical characteristic of a material, in the form of complex permittivity, impacts on the amount of power transmitted/reflected into/from a medium made of the same material.[26] In order to support the scientific research, the international space agencies, for example, NASA, replicated several Martian terrains thanks to some terrestrial analogs. An example of these studies is the JSC Mars-1, a Martian soil replicant obtained from the ash of the Pu'u Nene, which is a volcano located in Hawaii.[27] This was considered to be a Martian terrain analog due to its spectral similitude to the bright regions of Mars.[28] We considered it due to the huge amount of information in the literature about it, which has made possible a solid estimation of its complex permittivity. By expressing the complex permittivity as $\hat{\epsilon} = \epsilon_r' - i\epsilon_r''$, we can compute the real part ϵ' and the imaginary part ϵ'' thanks to the Cole–Cole equations:[29]

$$\epsilon' = \epsilon_\infty + (\epsilon_{DC} - \epsilon_\infty)\frac{1 + (\omega\tau)^{1-\alpha}\sin\alpha\pi/2}{1 + 2(\omega\tau)^{1-\alpha}\sin\alpha\pi/2 + (\omega\tau)^{2(1-\alpha)}}, \quad (1)$$

$$\epsilon'' = \frac{(\epsilon_{DC} - \epsilon_{\infty})(\omega\tau)^{1-\alpha} \cos \alpha\pi/2}{1 + 2(\omega\tau)^{1-\alpha} \sin \alpha\pi/2 + (\omega\tau)^{2(1-\alpha)}}, \tag{2}$$

with the angular velocity $\omega = 2\pi f$, the infinite and static dielectric permittivity defined as ϵ_∞ and ϵ_{DC}, the relaxation time constant τ, and the Cole–Cole distribution α. The frequency dependence of this computation will be analyzed later through results by initializing the Cole–Cole equations with the parameters value in Stillman and Olhoeft.[30]

3.1.3 | Fresnel coefficients

The estimate of the complex dielectric permittivity $\hat{\epsilon}$ is needed in order to understand the amount of power that will be "dissipated" during RF propagation. This is due to the scattering of the electromagnetic signal caused by the outdoor environment. Indeed, when the signal has a wavelength λ comparable to the dimension of an object, which is obstructing its propagation—a Martian rock or cliff, the so-called transmission and reflection phenomena happen. Transmission is meant the power transmitted T and lost into the medium, while reflection is the phenomena from which the incident power I is reflected (R) from the medium. In this case of study, the reflected power characterizes the power of the signal replica generated from the collision with the terrain along with the increased distance with respect the LOS. As we will see later, the ray traveling from TX to RX experiences a reflection when hitting a tile of the 3D structure. This means that only a percentage of the total amount of power incident to the interface will be redirected to another tile composing the terrain, while the transmitted power into the medium will be dissipated.

Thanks to the Fresnel coefficients and remembering the classical EM theory, where the incident power is $I = T + R$, we are able to compute the transmitted $T_{TE,TM}$ and reflected $R_{TE,TM}$ power, where the formulation is reported in the work provided in[31]

$$T^{TE} = abs\left(\frac{\left(1-\gamma^2\right)\cdot e^{\left(-i\left(\frac{2\pi}{\lambda}\cdot w_{area}\left(\sqrt{\hat{\epsilon}-sin^2(\theta_l)}-1\right)\right)\right)}}{\left(1-\gamma^2 e^{-2i\left(\frac{2\pi}{\lambda}\cdot w_{area}\cdot\sqrt{\hat{\epsilon}-sin^2(\theta_l)}\right)}\right)}\right) \quad \text{with} \quad \gamma = \left(\frac{cos(\theta_l) - \sqrt{\hat{\epsilon}-sin^2(\theta_l)}}{cos(\theta_l) + \sqrt{\hat{\epsilon}-sin^2(\theta_l)}}\right), \tag{3}$$

$$T^{TM} = abs\left(\frac{\left(1-\kappa^2\right)\cdot e^{\left(-i\left(\frac{2\pi}{\lambda}\cdot w_{area}\left(\sqrt{\hat{\epsilon}-sin^2(\theta_l)}-1\right)\right)\right)}}{\left(1-\kappa^2 e^{-2i\left(\frac{2\pi}{\lambda}\cdot w_{area}\cdot\sqrt{\hat{\epsilon}-sin^2(\theta_l)}\right)}\right)}\right) \quad \text{with} \quad \kappa = \left(\frac{\hat{\epsilon}\cdot cos(\theta_l) - \sqrt{\hat{\epsilon}-sin^2(\theta_l)}}{\hat{\epsilon}\cdot cos(\theta_l) + \sqrt{\hat{\epsilon}+sin^2(\theta_l)}}\right), \tag{4}$$

where θ_l is the angle of incidence, $\lambda = c/fm$ is the wavelength, c is the speed of light, and w_{area} is the thickness of the terrain. Indeed, we decided to compute the Fresnel coefficients by considering a thickness dependence of the attenuation introduced by the medium in order to simulate the width of the area, which otherwise would be infinitesimal.

The transmission power lost into the medium, which is characterized by a thickness w_{area}, is simply subtracted from the unitary power, to reduce the increase of the computational load, thus obtaining the reflected one $R_{TE,TM} = 1 - T_{TE,TM}$.

3.1.4 | 3D ray tracing

We started from the work provided by Hosseinzadeh[32] and well explained in Hosseinzadeh et al.[33] Hosseinzadeh et al. studied the propagation of the LoRa modulation by considering an indoor environment. They compared the performance of nondeterministic models, such as International Telecommunication Union (ITU) and log-distance, with deterministic ones, for example, multiwall and ray-tracing models. From the results, they found that for the estimation of the LoRa propagation, the best choice was the multiwall model in terms of accuracy, similar to the one obtained with the ray-tracing model, and reduced computational load with respect ray tracing. However, this is not true when dealing with strong small-scale fading, as correctly highlighted in Hosseinzadeh et al.[33] Thus, a 3D ray-tracing algorithm is recommended when the objective is the overall characterization of propagation impairments, especially over outdoor environments, although the computational complexity is really high and can be a limit, especially thinking to the required simulation time. The ray-tracing algorithm is based on geometrical optics as in McKown and Hamilton,[34] and it implements the procedures clearly shown in Figure 5. As briefly introduced before, it takes as input the 3D structure, or tile area, modeled on the basis of the DEM. It is iterated for the number of RXs that we choose to displace on the 3D tile area. Furthermore, it would be possible to consider multiple transmitter simply by iterating the process for the number of TXs and adapting the various matrices dimensions. However, this will not be considered in this work, but it will be subject of future analysis.

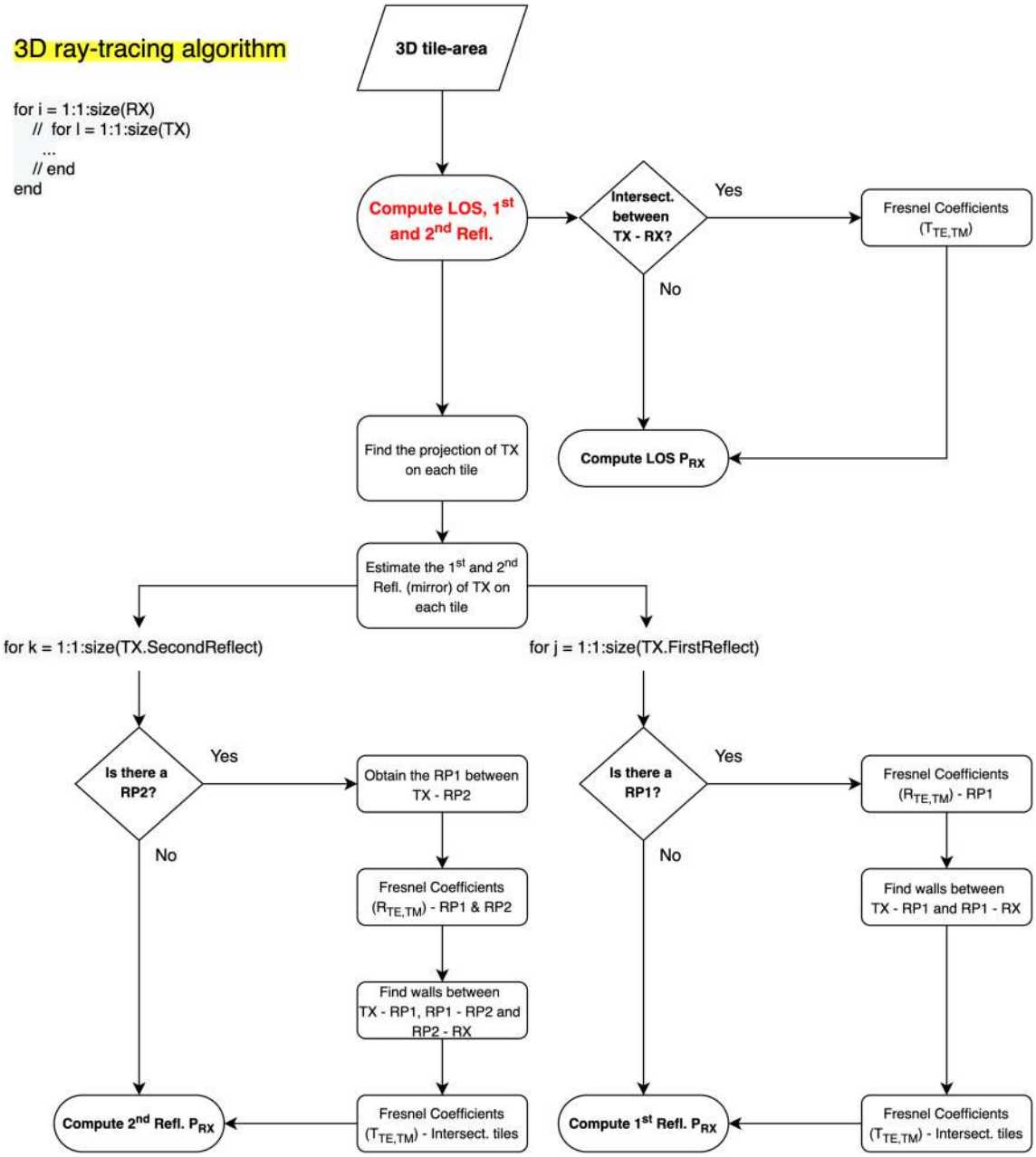

FIGURE 5 Flowgraph of the 3D ray-tracing algorithm for outdoor environment

First, it traces the LOS with the aim of finding the received power of the signal in the location where the RX is placed. Obviously, between TX and RX, there can be rocks or cliffs obstructing the LOS and dissipating power in the terrain. Thus, we find the intersection between TX and RX in order to account for the power lost, thanks to the Fresnel coefficients, into the medium as follows:

$$P_{LOS}^{dBW} = P_{TX}^{dBW} - 10log_{10}\left(\frac{4\pi d_{TX,RX}}{\lambda}\right)^2 + 10log_{10}(T_{TX,RX}^{TE,TM}) + G_{TX}^{dBW} + G_{RX}^{dBW}, \tag{5}$$

where $d_{TX,\,RX}$ is the distance between TX and RX, $10log_{10}(T_{TX,RX}^{TE,TM})$ is the power lost in dB with $0 < T < 1$, and G_{TX}^{dBW} and G_{RX}^{dBW} are the TX and RX antenna gains. Now, the power of the first reflections and second reflections are needed to obtain the total received power at the RX side and to analyze the effect of the small-scale phenomena on the propagation. For the sake of completeness, the first reflection means the path traveled by the signal which is reflected only one time from a reflection point (RP) before reaching the RX, while the second reflection is the replica of the signal which arrives to the RX by reflecting on two RPs. The algorithm finds the projection of TX on each tile, thus allowing to estimate the

reflections, or mirrors, of the selected TX on each tile composing the 3D structure. The power of the first reflection is computed by searching for the RP1 characterizing the path between TX and RX. If there is actually a RP1, the "ray tracer" proceeds to the computation of the reflection coefficients in order to estimate the amount of reflected power from the RP1. Then, it finds the walls between the path TX-RP1 and RP1-RX by understanding the amount of power transmitted into each intersecting tiles. The received power due to the first reflection is based on the following equation:

$$\begin{aligned} P_{1^{st}Refl}^{dBW} &= P_{TX}^{dBW} - 20log_{10}\left(\frac{4\pi d_{TX,RP_n} + d_{RP_n,RX}}{\lambda}\right) + 10log_{10}(T_{TX,RP_n}^{TE,TM}) \\ &+10log_{10}(R_{RP_n}^{TE,TM}) + 10log_{10}(T_{RP_n,RX}^{TE,TM}) + G_{TX}^{dBW} + G_{RX}^{dBW}. \end{aligned} \tag{6}$$

The second reflections are evaluated through the same process of the first with the exception that, if there is a RP2, we need to obtain the RP1 between TX-RP2. Then, two RPs mean that we will have to compute the reflected power from the RP1 and RP2, as well as finding the tiles, or walls, intersecting the paths TX-RP1, RP1-RP2, and RP2-RX. The transmission coefficients are estimated for each intersection, and the power of the second reflection is based on the following computation:

$$\begin{aligned} P_{2^{nd}Refl}^{dBW} &= P_{TX}^{dBW} - 20log_{10}\left(\frac{4\pi d_{TX,RP_n} + d_{RP_n,RP_{n+1}} + d_{RP_{n+1},RX}}{\lambda}\right) + 10log_{10}(T_{TX,RP_n}^{TE,TM}) \\ &+10log_{10}(R_{RP_n}^{TE,TM}) + 10log_{10}(T_{RP_n,RP_{n+1}}^{TE,TM}) + 10log_{10}(R_{RP_{n+1}}^{TE,TM}) + 10log_{10}(T_{RP_{n+1},RX}^{TE,TM}) + G_{TX}^{dBW} + G_{RX}^{dBW}. \end{aligned} \tag{7}$$

3.1.5 | Post-process and other propagation impairments

The knowledge coming out from the "ray tracer" allows us to process data for the analysis of large-scale and small-scale phenomena. Moreover, as introduced in Section 2, we can integrate the formulation representing other propagation impairments about atmosphere, cloud and fog, aerosol, and dust storm attenuation, which are not directly studied through the main algorithm, in order to get a complete overview of the effect altering the RF propagation. The first analysis that should be made is the computation of the outage probability, which is the probability of having a completely blocked RF propagation due to big obstacles, such as big rocks and cliffs, obstructing the signal. This can be easily approximated by imposing a threshold on the minimum detectable signal (MDS), which is defined as follows:

$$MDS(dBm) = 10 \cdot log_{10}(k \cdot T \cdot 1000) + NF^{dB} + 10 \cdot log_{10}(B_w), \tag{8}$$

where k is the Boltzmann's constant, T is the temperature in K, NF is the noise figure expressed in dB, and B_w is the receiver bandwidth. Then, by counting the occurrence of the samples below the threshold, in terms of received power P_{RX}, the percentage representing the blocking probability is obtained. From the data regarding the received power and the distance traveled from the LOS, first reflection, and second reflection, we can estimate, in a first instance, the RMS delay spread σ_τ, which is defined as shown here below:[35]

$$\sigma_\tau = \sqrt{\overline{\tau^2} - (\overline{\tau})^2} \text{ with } \overline{\tau^2} = \frac{\sum P(\tau_k)\tau_k^2}{\sum P(\tau_k^2)} \text{ and } \overline{\tau} = \frac{\sum P(\tau_k)\tau_k}{\sum P(\tau_k)}, \tag{9}$$

where $\tau = \frac{d_{Refl.} - d_{LOS}}{c}$ is the path delay of the jth signal replica, with c the speed of light, d_{LOS} the path traveled by the LOS, and $d_{Refl.}$ the distance traveled by the jth signal replica. For what concerns the PDP, in order to get the behavior for which the path replicas are attenuated as the delay with respect the LOS increases, the *Curve Fitting Toolbox* of Matlab can be exploited to fit the attenuation of each path replica and estimate a PDP analytical model.[10] The received power of the samples representing the LOS (P_{LOS}), for a certain distance between TX and RX and over precise Martian locations, can be used to derive a path loss exponent value, similar to what is done in Bonafini and Sacchi.[9] By varying the path loss exponent p in the following equation, we can fit the gathered samples and estimate an average path loss exponent for our results:

$$L(d) = \left(\frac{4\pi d_{TX,RX}}{\lambda}\right)^p. \tag{10}$$

Moreover, the standard deviation of the LOS received power gives us an indication of the fluctuation of the power, due to the morphology of the area in which we are simulating, around the mean, that is, the shadowing effect.

Other kind of attenuation, that is, the ones cited above, can be accounted by referring to the formulation and data found in NASA.[22,23] For example, the attenuation due to cloud and fog can be accounted by applying the following equation:

$$k_i = 0.4343\frac{6\pi}{\lambda} Im\left[-\frac{K_c - 1}{K_c + 2}\right], \tag{11}$$

where k_i is the attenuation coefficient (dB/km/gm/m^3) and K_c is the complex dielectric permittivity of water or ice.[22] Instead, dust storms attenuation can be expressed as follows:

$$A_{DS}(\lambda) = \frac{1.029 \times 10^6 \varepsilon''}{\lambda \cdot [(\varepsilon' + 2)^2 + \varepsilon''^2]} N_T \bar{r}^3, \tag{12}$$

where the real and imaginary part of the dielectric permittivity of dust particles are ε' and ε'', the total particle density for m^3 is N_T, and the mean particle radius, expressed in m, is $\bar{r}$.[23] Finally, by considering the ITU model about large-scale atmospheric attenuation, which is implemented in Matlab through the *gaspl* function, we can roughly estimate the attenuation on the propagation introduced by the Martian atmosphere.[36]

3.2 | Simulation workflow

The simulator follows various steps in order to finally estimate statistically relevant and solid Martian channels to be used for testing of network infrastructures and communication systems. Indeed, with this work, we aim to provide a tool through which it will be possible to correctly initialize software, such as GNU Radio, LabVIEW, Simulink, and Matlab, mostly for the evaluation of performance at data link and PHY-layer side. In Figure 6, we show how the simulator is designed. As visible, the first step was the selection of the DEM representing the Gale crater to be used

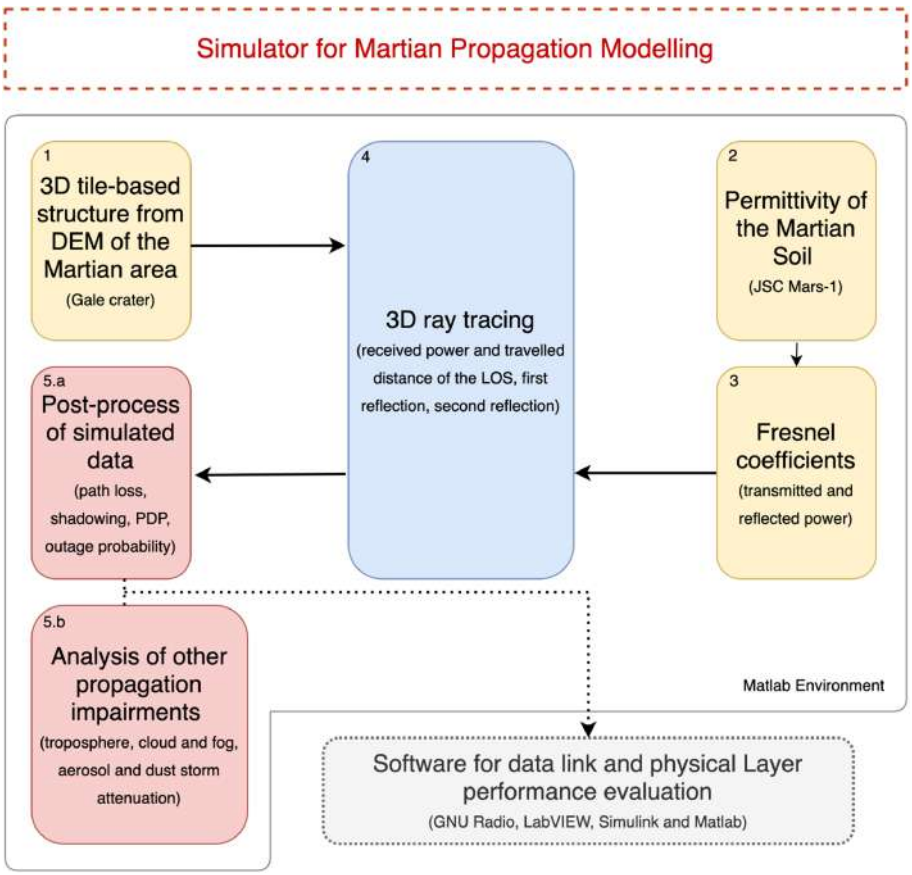

FIGURE 6 Flowgraph of the developed simulator showing all the Steps from 1 to 5.a and 5.b for the evaluation of Martian propagation phenomena

as input for the 3D ray-tracing algorithm. The DEM is modeled to construct a 3D structure in Matlab to be used for simulating the RF propagation (*Step 1*). Then, we estimated the permittivity of a possible Martian soil, for example, the Martian replicant soil JSC Mars-1, thanks to the Cole–Cole equations in order to electrically characterize the 3D structure. The complex permittivity value coming out from *Step 2* is imported in the computation of the Fresnel coefficients. Consequently, we are able to understand the amount of power transmitted/reflected into/from the medium, that is, the Martian soil (*Step 3*). At this time, the 3D ray-tracing algorithm comes into play by tracing the LOS, first reflection, and second reflection of an RF signal sent from one specific location to another over the 3D structure (*Step 4*). The Fresnel coefficients allow considering not only the distance traveled by each signal replicas over the terrain but also accounting for the power lost due to the incidence of the signal on the terrain. The information about the number of generated signal replicas, the received power of each signal replicas, and the LOS, the total received power in a certain location, and the path delays with respect to the LOS are put as input to the post-process script, which computes path losses, shadowing values, outage probability, and PDPs. From both *Steps 5.a* and *5.b*, where we analyze through the propagation impairments due to the troposphere, clouds and fogs, aerosol, and dust storms, we estimate a complete framework describing the effect of Mars on the RF propagation. These data become relevant when dealing with the modeling of statistical channels in commercial software as the ones cited above.

4 | RESULTS

The implementation of the model, that we proposed in the previous section, will be accompanied by a collection of results spreading from the large-scale and small-scale phenomena to the computation of the outage probability, that is, the probability of experimenting a blockage in the transmission. Moreover, to characterize the results, first, we will analyze the environment, thus the GA1 and GA2, from a statistical perspective. This will give us the dimension of the gathered data, in the sense that we will better understand and contextualize the results. We will start by showing the samples regarding the LOS and the estimated signal replicas for each subarea (SA). Then, we will compute the blocking probability for each SA, a discussion that will be linked to the intrinsic morphology of the SA. Large-scale phenomena and small-scale phenomena will be studied by averaging the whole amount of realization for each SA, thus focusing on the overall area. We considered transmissions with a euclidean distance between TX and RX $d_{TX,RX} = \{100, 200\}$, which represents the radius of common terrestrial picocells. We selected all the possible locations distant $d_{TX,RX}$ from the TX, which is located in the origins of the Cartesian coordinate system. To conclude, we initialized the model with the working frequencies $f = \{2.5, 39.0\}$ GHz, that is, S band and EHF band, respectively, that are indicated by Verizon as carrier frequencies of the terrestrial 5G. Everything is designed, implemented, and analyzed thanks to Matlab.

4.1 | Simulated testing environment

As written in Section 3.1.1, we took the DEM of the Gale crater with a resolution of 1 m/px. We cropped it into two areas of 1000 × 1000 m, a flat one and a rocky one, called, respectively, GA1 and GA2, depicted in Figure 3A,B. We downsampled them in order to decrease the impact in terms of computational load, which is one of the major drawback of the 3D ray tracing. The areas are divided along the diagonals into eight SAs, each one with a side length of 250 m. It is interesting to characterize mathematically these SAs through common statistical measures, as mean and standard deviation, and the gradient operation, which is already shown in Figure 2B and better highlights the slopes of the Gale crater. From Tables 1 and 2, it is easily demonstrated the deep heterogeneity of the areas, both globally and locally. The GA1 is situated −4500 m below the "sea" level, while the GA2 is located on the rise of the Gale crater central peak at more or less −3100 m. However, the SAs of the GA2 extend from −3235.5 to −3071.8 m. As we can see, the maximum gradient for the GA2 is the one of the SA3, which is 98.64 m of excursion, while for

TABLE 1 Statistical representation of the "Gale Crater—Area 1" morphology

Subarea|"Gale Crater—Area 1"	Mean elevation (m)	Maximum gradient (m)	Standard deviation (dB)
Subarea 1	−4499.2	13.57	4.98
Subarea 2	−4500.3	10.18	2.25
Subarea 3	−4500.8	6.56	1.54
Subarea 4	−4499.0	11.80	3.84
Subarea 5	−4501.4	8.03	2.30
Subarea 6	−4502.9	5.86	1.23
Subarea 7	−4499.7	5.80	0.56
Subarea 8	−4497.1	10.50	3.68

Note: Standard deviation stands for the fluctuation around the mean elevation.

TABLE 2 Statistical representation of the "Gale Crater—Area 2" morphology

Subarea|"Gale Crater—Area 2"	Mean elevation (m)	Maximum gradient (m)	Standard deviation (dB)
Subarea 1	−3235.5	34.44	8.15
Subarea 2	−3196.2	85.45	13.54
Subarea 3	−3149.2	98.64	13.98
Subarea 4	−3071.8	82.83	11.31
Subarea 5	−3193.7	88.01	12.69
Subarea 6	−3199.4	84.64	12.88
Subarea 7	−3157.6	84.00	12.77
Subarea 8	−3168.9	88.94	12.79

Note: Standard deviation stands for the fluctuation around the mean elevation.

the GA1, the maximum value is 13.98 m of the SA1. From this and from the standard deviation of each SA for both the areas, we can expect severe alterations on the RF propagation for the GA2, which results to be really rocky and steep with respect the GA1. This will especially be evident in terms of path loss exponent, shadowing, and overall outage probability; indeed, big obstacles are the major contributions of these effects for what concerns the degradation of the signal.

4.2 | Propagation impairments

We iterated 64 times the model in order to initialize the system with $f = \{2.5, 39.0\}$ GHz and $d_{TX,RX} = \{100, 200\}$ for each SA composing GA1 and GA2. As discussed before and visible from Figure 6, we need to estimate the complex permittivity for the chosen frequency in order to compute the Fresnel coefficients and estimate the transmitted and reflected power into/from the terrain. In order to do that, we exploited the values in Stillman and Olhoeft[30] for the JSC Mars-1, where $\rho = 1.60$ (g/cm^3), $\epsilon_\infty = 5.30$, $\epsilon_{DC} = 2.86$, $\tau_\infty = 9.3 \times 10^{-5}$, $E = 0.175$ (eV), $\alpha = 0.13$, and $\mu_r 1.00$. Thus, the complex permittivity is defined as $\hat{\epsilon}(2.5\text{GHz}) = 2.90 - 0.15i$ and $\hat{\epsilon}(39.0\text{GHz}) = 2.87 - 0.01i$.

Where demanded, we considered an average Martian temperature $T = 210$ K, which is equal to -63° C.[37] Clearly, this is a generic assumption, which should be revised for further work by taking into account a certain fluctuation around the average temperature.

Now, let's see the gathered samples coming out from the "ray tracer." Figures 7 and 8 show the samples obtained for each SA of the GA1 and GA2. The samples related to the GA1 shows, especially from Figure 7D, few samples with a really low received power P_{RX} with respect to a free-space propagation. These values are concentrated on the SA2, SA3, SA5, and SA7. Very different is the situation of the GA2. Figure 8A shows samples well below the MDS (blue and red dotted lines), which will be defined in a while. For both the considered working frequencies, each SA presents very attenuated LOS propagation, except for the SA2, which from Table 2 results to be the terrain with the highest standard deviation. However, the statistical analysis does not consider the TX elevation with respect the RX. Indeed, if a TX is placed on a cliff and the RXs are situated on a valley, the transmission will not be affected by severe alterations due to the clearance of the Fresnel zone. This will be clear in the following discussion.

4.2.1 | Outage probability

The blue dotted line and the red dotted line in Figures 7 and 8 represent the MDS, where we considered for the $f = 2.5$ GHz a receiver bandwidth $B_w = 100$ MHz and for the $f = 39.0$ GHz $B_w = 400$ MHz.[38] These thresholds are $MDS(2.5\text{GHz}) = -117.23$ dB and $MDS(2.5\text{GHz}) = -111.21$ dB, which are used to count the samples of nondetectable signals at the RX side, thus computing the outage probability. Indeed, the outage probability is the phenomena describing the probability of not being able to detect the transmitted signal. Typically, it is mostly caused by the geometry of the environment in which the RF propagation happens, then, obviously, by the distance, which increasing increases also the probability of finding an obstruction, by the frequency (higher frequencies correspond to shorter wavelengths), and by the electrical properties of the environment. As expected, the distance acts on the probability of obstruction of the RF propagation, as well as the frequency. The data gathered for $f = 39.0$ GHz exhibits lower power, as understandable, with respect to the $f = 2.5$ GHz. The objects obstructing the RF propagation lead to higher amount of lost power for higher frequencies, thus lower wavelengths. However, the morphology of the terrain is the main actor on the increase of the outage probability. This is shown in Figure 9, where Figure 9D exhibits a blocking percentage of about 50% for the SA4. In the context of a communication systems working on such an environment, we will have one out of two possibilities of not being able to even detect the signal at RX side for, more or less, both frequencies and $d_{TX,RX} = 200$ m. Analyzing the SA8 of the GA2 for example, it is interesting to highlight that, despite the fact

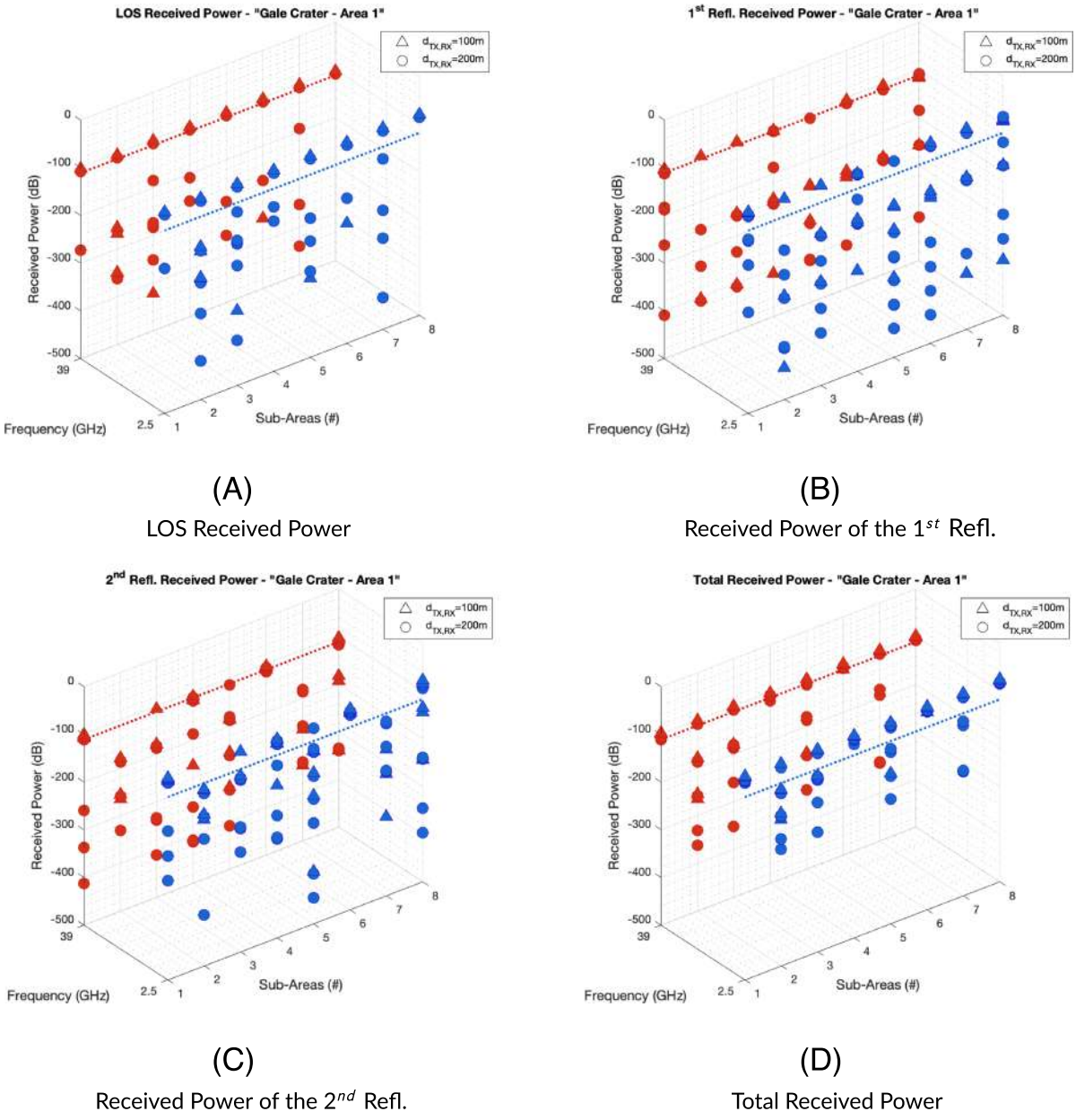

FIGURE 7 (A) LOS received power for the working frequency $f = \{2.5, 39.0\}$ GHz versus subareas composing the "Gale Crater—Area 1." (B) First reflection received power for the working frequency $f = \{2.5, 39.0\}$ GHz versus subareas composing the "Gale Crater—Area 1." (C) Second reflection received power for the working frequency $f = \{2.5, 39.0\}$ GHz versus subareas composing the "Gale Crater—Area 1." (D) Total received power for the working frequency $f = \{2.5, 39.0\}$ GHz versus subareas composing the "Gale Crater—Area 1"

of showing low outage probability with respect the other SAs, from Table 2, we see its maximum gradient of about 89m and the standard deviation of 12.79 dB, the third highest between the other SAs. However, the TX is placed in this case at −3140 m while the RXs at the two considered distances are displaced on a valley at −3200 m and a hill at −3160 m. This lead to that clearance of the Fresnel zone, that we briefly debated above, with respect to other cases, as for example the SA2 of the GA1, where we have lower gradient, lower standard deviation but still a higher outage probability.

4.2.2 | Large-scale phenomena

Large-scale phenomena attenuates the signal constantly over the whole bandwidth. Among them, we can indicate the path loss, which is the attenuation due to the wavelength and the distance traveled by the signal, the shadowing, that is, the fluctuation of the received power P_{RX}

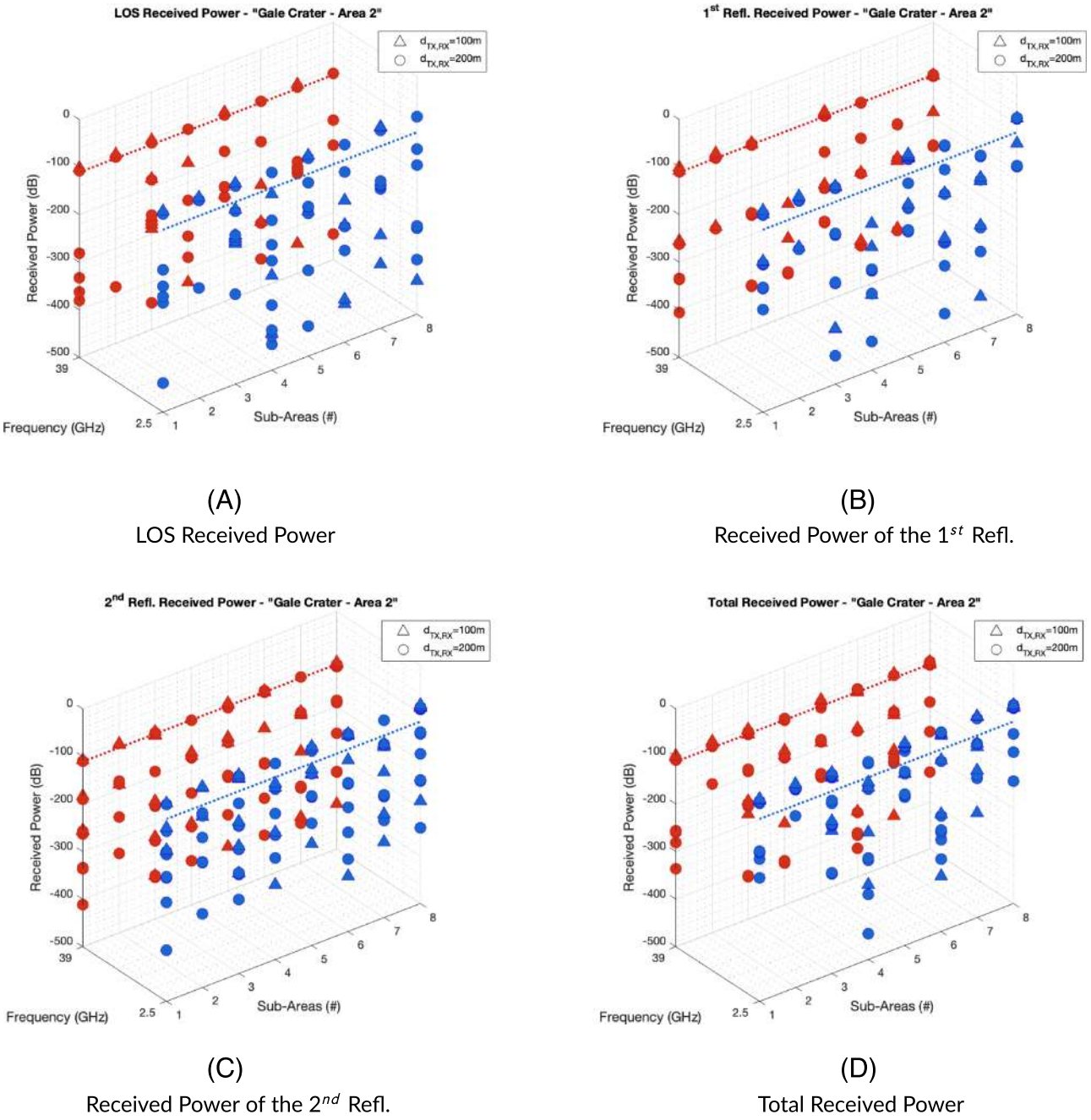

(A) LOS Received Power

(B) Received Power of the 1^{st} Refl.

(C) Received Power of the 2^{nd} Refl.

(D) Total Received Power

FIGURE 8 (A) LOS received power for the working frequency $f = \{2.5, 39.0\}$ GHz versus subareas composing the "Gale Crater—Area 2." (B) First reflection received power for the working frequency $f = \{2.5, 39.0\}$ GHz versus subareas composing the "Gale Crater—Area 2." (C) Second reflection received power for the working frequency $f = \{2.5, 39.0\}$ GHz versus subareas composing the "Gale Crater—Area 2." (D) Total received power for the working frequency $f = \{2.5, 39.0\}$ GHz versus subareas composing the "Gale Crater—Area 2"

among the mean, and the atmospheric attenuation. As discussed before, for Mars, we should consider also the attenuation due to the dust storms and to the clouds or fogs. This last term will not be treated in this work, except for the brief introduction in Section 3.1.5, because it was extensively described in NASA,[22] while the other values will be analyzed in the following paragraphs.

Path loss and shadowing

We took the received powers P_{RX} for each signal samples acquired over the GA1 and GA2 and averaged them in order to characterize the propagation for each SA. The path loss exponents were then obtained by fitting the P_{RX} of the ith realization with the path loss value computed by iterating the exponent p in Equation (10) between [1.8 : 0.01 : 4]. Tables 3 and 4 refer, respectively, to the GA1 and GA2. Here, the morphology of

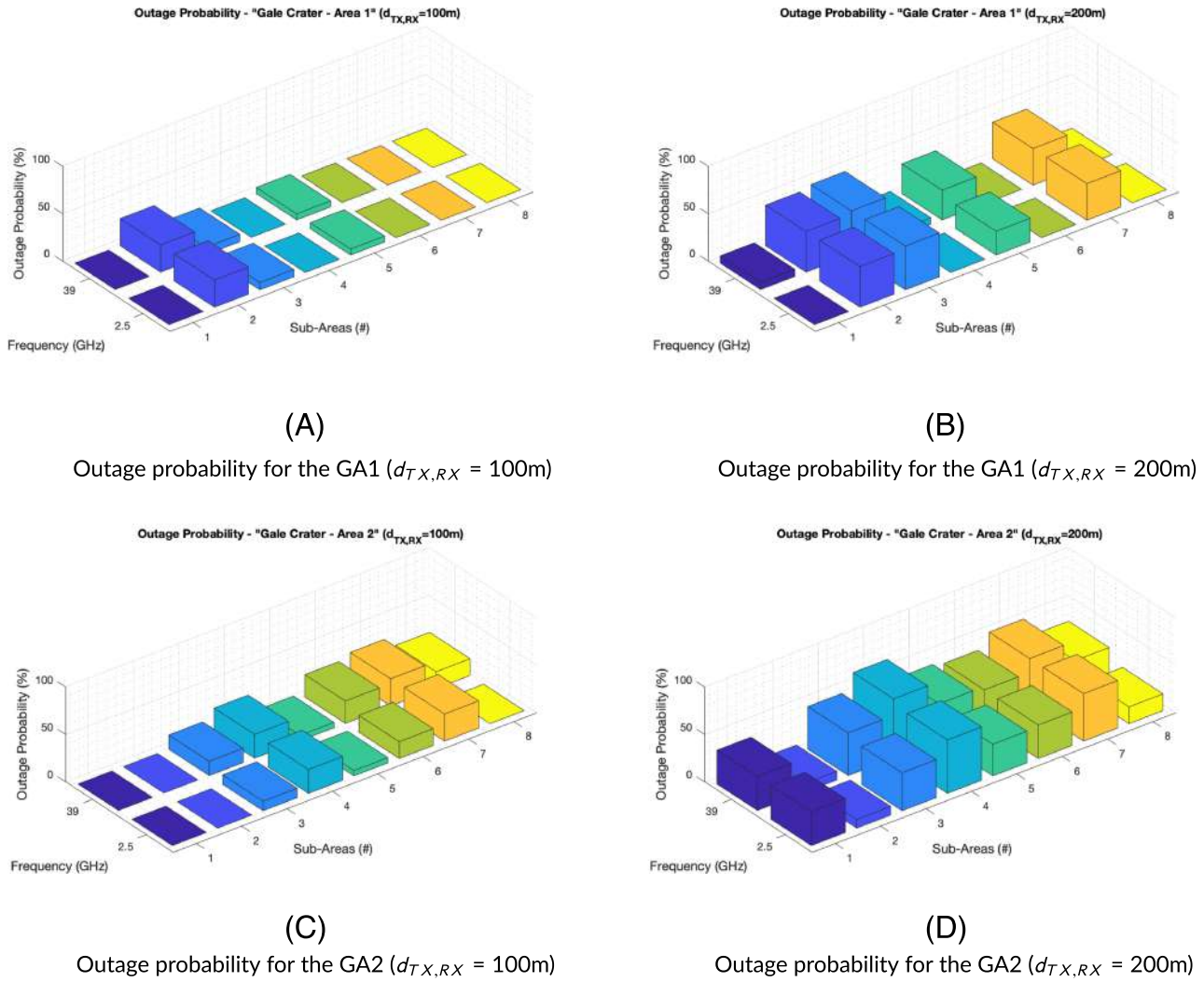

FIGURE 9 (A) LOS received power for the working frequency $f = \{2.5, 39.0\}$ GHz versus subareas composing the "Gale Crater—Area 1." (B) First reflection received power for the working frequency $f = \{2.5, 39.0\}$ GHz versus subareas composing the "Gale Crater—Area 1." (C) Second reflection received power for the working frequency $f = \{2.5, 39.0\}$ GHz versus subareas composing the "Gale Crater—Area 2." (D) Total received power for the working frequency $f = \{2.5, 39.0\}$ GHz versus subareas composing the "Gale Crater—Area 2"

TABLE 3 Estimated path loss exponent and shadowing effect for the "Gale Crater—Area 1"

"Gale Crater—Area 1"	Mean PL exponent	Maximum PL exponent	Minimum PL exponent	Standard deviation (dB)
$f = 2.5$ GHz	1.99	2.11	1.95	3.69
$f = 39.0$ GHz	2.00	2.09	1.96	3.70

Note: Standard deviation is computed on the logarithmic value of the LOS over each terrain.

TABLE 4 Estimated path loss exponent and shadowing effect for the "Gale Crater—Area 2"

"Gale Crater—Area 2"	Mean PL exponent	Maximum PL exponent	Minimum PL exponent	Standard deviation (dB)
$f = 2.5$ GHz	2.63	4.56	1.96	11.79
$f = 39.0$ GHz	2.57	3.87	1.97	11.99

Note: Stdandard deviation is computed on the logarithmic value of the LOS over each terrain.

the two areas strongly acts on the received power by heavily reducing it in the case of a rocky and steep environment, such as the GA2. Indeed, the GA1, from our estimation, is characterized by an average path loss exponent of about 2, which basically is the FSPL. This is something expected just by visualizing the area in Figure 3A. The lack of big rocks and cliffs lead to such kind of RF propagation. Instead, Table 4 exhibits higher path loss exponents. The mean is around 2.6, which is near to the path loss exponent of a terrestrial urban area. Furthermore, with respect

the GA1, the shadowing value is way stronger reaching ∼12 dB. The fluctuation of the received power, which is so really evident, is due to the big obstacles, in form of big rocks and cliffs, obstructing the free propagation.

Atmosphere and dust storms

For what concerns these kinds of attenuation, we exploited, first, the *gaspl* function, which is integrated in Matlab. It performs the atmospheric gas attenuation model of the ITU.[36] The atmospheric attenuation is primarily caused by oxygen and water vapor. Thus, by initializing the *gaspl* function with an average surface pressure of 610 Pa[39] and the water vapor density of 0.0013 g/m^3,[40] we can roughly estimate the spectral resonance of the atmospheric attenuation on Mars. Figure 10A shows a peak at around 25 GHz, which is mostly due to the water vapor, while between 60 and 70 GHz, we have the highest attenuation caused by the oxygen molecules, as also similarly achieved in NASA.[41] As we can see, as the distance between TX and RX increases, the attenuation increases too following a logarithmic behavior.

Although this model is not perfectly fitted to the Martian environment—being a terrestrial model and not considering the most recurrent gas in the atmosphere of Mars (carbon dioxide and nitrogen), it gives us an indication on the severe atmospheric attenuation for certain frequencies. $f = \{2.5, 39.0\}$ GHz are not affected by the spectral resonance of the H20 and 02, which can cause 30 dB of attenuation for a path of 10 km and a working frequency between 60 and 70 GHz. Thus, they can be used as working frequencies of ad hoc communication systems without particular problems for what concerns atmospheric attenuation. Moreover, for cellular networks with dimensions of hundreds of meters, the atmospheric attenuation are negligible.

The attenuation led by dust storms was computed upon the formulation of Equation (12) and considering the complex permittivity of the JSC Mars-1, which varies with frequency. Figure 10B shows that with the increase of frequency, the attenuation in dB/km remains, more or less, constant. However, as we consider a higher particle radius, we experiment a solid increase in the attenuation up to 0.055 dB/km. For sizes of picocells, it should be irrelevant but for longer paths, and taking into account that dust storms can cover the whole Mars, it is for sure a term that negatively affects the RF propagation.

4.2.3 | Small-scale phenomena

The multipath fading refers to rapid fluctuations in the received signal, which causes constructive or destructive interference and shifts in the signal phase. This is due to the multiple paths that the signal travels in order to reach the RX. These paths are generated by the collisions of the signal with the environment surrounding it. Indeed, big obstacles reflect the propagation to other RPs, which reflect the signal another time until, with a certain probability, it reaches its destination.

The multipath fading is then modeled through the formulation expressed by Equation (9), where the RMS delay spread σ_τ expresses the difference in time between the first and last arrived signal replica. However, in this brief last discussion, we decided to concentrate on the needed values in order to model the multipath channel. Thus, in Tables 5 and 7, we present the average, maximum, and minimum delays experimented

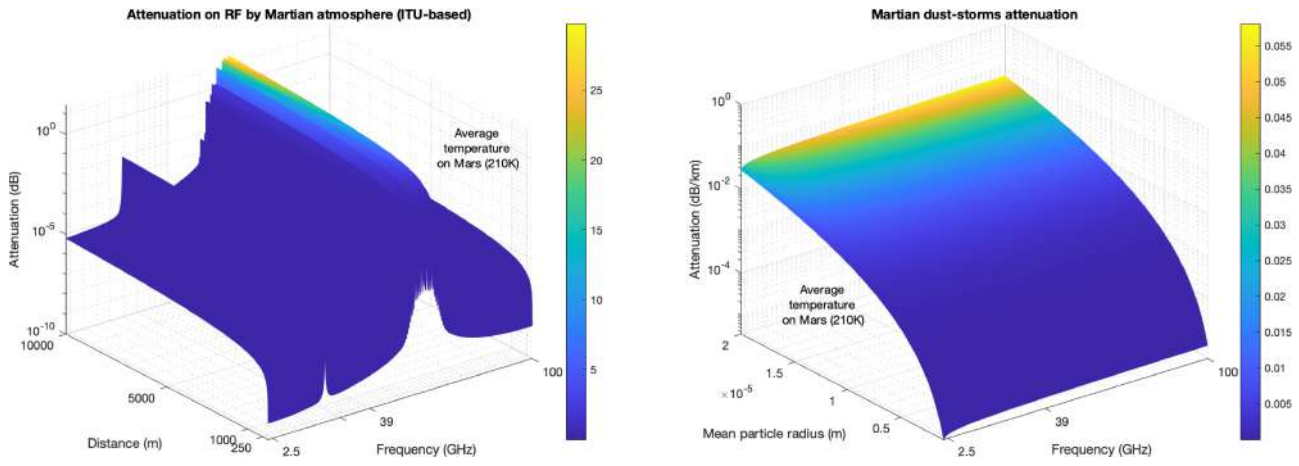

(A) Atmospheric Attenuation

(B) Dust-Storm Attenuation

FIGURE 10 (A) Attenuation due to Martian atmosphere for a frequency span between 1 and 100 GHz versus distance. (B) Attenuation due to Martian dust storms for a frequency span between 1 and 100 GHz versus mean particle radius N_T

TABLE 5 Statistical representation of the path delays generated due to the first and second signal reflections over the "Gale Crater—Area 1"

"Gale Crater—Area 1"	Mean delay (s)	Maximum delay (s)	Minimum delay (s)	Standard deviation
First Refl. ($d_{TX,RX} = 100$ m)	5.47e-07	8.11e-07	3.40e-07	1.86e-07
Second Refl. ($d_{TX,RX} = 100$ m)	9.85e-07	1.16e-06	7.79e-07	1.45e-07
First Refl. ($d_{TX,RX} = 200$ m)	7.76e-07	8.34e-07	7.37e-07	3.50e-08
Second Refl. ($d_{TX,RX} = 200$ m)	9.78e-07	1.11e-06	8.23e-07	1.05e-08

Standard deviation is computed on the mean path delays characterizing each subarea.

TABLE 6 Statistical representation of the path attenuation generated due to the first and second signal reflections over the "Gale Crater—Area 1"

"Gale Crater—Area 1"	Mean P_{RX} (W)	Maximum P_{RX} (W)	Minimum P_{RX} (W)	Standard deviation
First Refl. ($d_{TX,RX} = 100$ m, $f = 2.5$ GHz)	1.76e-09	4.34e-09	2.73e-19	1.53e-09
Second Refl. ($d_{TX,RX} = 100$ m, $f = 2.5$ GHz)	2.82e-10	5.35e-10	4.08e-20	2.37e-10
First Refl. ($d_{TX,RX} = 200$ m, $f = 2.5$ GHz)	5.45e-10	1.31e-09	7.49e-21	6.12e-10
Second Refl. ($d_{TX,RX} = 200$ m, $f = 2.5$ GHz)	1.99e-10	4.62e-10	1.80e-15	2.16e-10
First Refl. ($d_{TX,RX} = 100$ m, $f = 39.0$ GHz)	8.33e-12	1.78e-11	2.28e-26	6.56e-12
Second Refl. ($d_{TX,RX} = 100$ m, $f = 39.0$ GHz)	2.64e-12	6.48e-12	9.39e-28	2.91e-12
First Refl. ($d_{TX,RX} = 200$ m, $f = 39.0$ GHz)	1.59e-12	3.70e-12	3.95e-27	1.37e-12
Second Refl. ($d_{TX,RX} = 200$ m, $f = 39.0$ GHz)	9.29e-13	2.24e-12	4.82e-20	9.88e-13

Note: Standard deviation is computed on the mean path attenuation characterizing each subarea.

TABLE 7 Statistical representation of the path delays generated due to the first and second signal reflections over the "Gale Crater—Area 2"

"Gale Crater—Area 2"	Mean delay (s)	Maximum delay (s)	Minimum delay (s)	Standard deviation
First Refl. ($d_{TX,RX} = 100$ m)	5.06e-07	8.41e-07	4.03e-07	1.73e-07
Second Refl. ($d_{TX,RX} = 100$ m)	7.36e-07	9.09e-07	6.14e-07	1.14e-07
First Refl. ($d_{TX,RX} = 200$ m)	7.60e-07	8.54e-07	7.02e-07	5.26e-08
Second Refl. ($d_{TX,RX} = 200$ m)	9.77e-07	1.10e-06	9.10e-07	7.60e-08

Note: Standard deviation is computed on the mean path delays characterizing each subarea.

over the GA1 and GA2, while, in Tables 6 and 8, we estimate the mean, maximum, and minimum received power for the considered distances, frequencies, and areas. Furthermore, the standard deviation depicts the dispersion of the sample delay and attenuation around the reported mean. Comparing Tables 5 and 7, we notice a stronger mean delay for what concerns the GA2 with respect to the GA1. The rocky area increases the possibility of having RPs between TX and RX, thus creating longer paths. The same behavior can be found when dealing with the received power $P(j)_{RX}$ of the jth replica. The nature of the GA2 impacts on the received power by, overall, lowering it, compared to the values gathered for the GA1. If we take a look to the $min(\overline{P}_{RX})$ (fourth column of Tables 6 and 8), the values are generally well below the MDS. From this, we get that such replicas do not impact on the demodulation process of the signal at the receiver side, because they are not even discernible, both for the GA1 and GA2.

The parameters on the tables can be exploited to model possible Martian channels. For example, it is possible to model channels made of six path replicas, divided into three first reflections and three second reflections from Tables 5 and 7, which are associated to the received power values in Tables 6 and 8. By normalizing the received power of the signal replicas, the PDP can be easily obtained for the two considered distances, frequencies, and areas. The attention should be, however, put to the minimum received power, in order to take into account the MDS, previously detailed. This will not be covered by this work, but it will be matter of study of future analysis.

4.3 | Limitations

There are few limitations, which are fair to point out. First, the model has a sensible impact on the computational load. For this reason, we limited our analysis to few distances between TX and RX and we downsampled by a factor of 5 the DEM's resolution. However, this was only a matter of

TABLE 8 Statistical representation of the path attenuation generated due to the first and second signal reflections over the "Gale Crater—Area 2"

"Gale Crater—Area 2"	Mean P_{RX} (W)	Maximum P_{RX} (W)	Minimum P_{RX} (W)	Standard deviation
First Refl. ($d_{TX,RX} = 100$ m, $f = 2.5$ GHz)	1.89e-09	3.55e-09	9.00e-21	1.65e-09
Second Refl. ($d_{TX,RX} = 100$ m, $f = 2.5$ GHz)	4.14e-10	1.28e-09	3.70e-15	4.82e-10
First Refl. ($d_{TX,RX} = 200$ m, $f = 2.5$ GHz)	9.64e-12	1.79e-11	1.69e-27	7.74e-12
Second Refl. ($d_{TX,RX} = 200$ m, $f = 2.5$ GHz)	2.13e-12	6.89e-12	1.44e-19	2.58e-12
First Refl. ($d_{TX,RX} = 100$ m, $f = 39.0$ GHz)	2.98e-10	7.21e-10	2.81e-30	2.84e-10
Second Refl. ($d_{TX,RX} = 100$ m, $f = 39.0$ GHz)	7.20e-11	1.22e-10	3.76e-15	4.39e-11
First Refl. ($d_{TX,RX} = 200$ m, $f = 39.0$ GHz)	1.36e-12	2.96e-12	9.84e-42	1.21e-12
Second Refl. ($d_{TX,RX} = 200$ m, $f = 39.0$ GHz)	4.40e-13	6.77e-13	8.36e-20	2.53e-13

Note: Standard deviation is computed on the mean path attenuation characterizing each subarea.

time; indeed, further work will broaden the study by considering longer path lengths. Moreover, we put the thickness of the area equal to the DEM's resolution in order to give depth to our 3D structure. This is clearly an approximation for what concerns the computation of the Fresnel coefficients and the amount of transmitted and reflected power. However, it was done to not increase even more the complexity of the system, thus the time required for the simulations. To conclude, the electrical analysis, which characterizes the Martian soil in terms of frequency-dependent complex permittivity, is based on the JSC Mars-1, actually a replicant of a possible Martian sediment. Although a certain degree of approximation is introduced, this was the best choice from our perspective as samples of Mars soil have not yet returned back to Earth. Further work will be addressed at improving and refining our simulator, while also optimizing the trade-off between complexity and performance.

5 | CONCLUSIONS

This paper has provided the tools for implementing a simulator for the understanding of the RF propagation over Mars thanks to high-resolution DEMs and a 3D ray-tracing algorithm. We deeply detailed each followed step for the design of the model, and the results were analyzed in terms of large-scale and small-scale phenomena. Moreover, we outlined a way for the computation of the outage probability, which is a really relevant term when developing and parameterizing ad hoc communication systems. Achieved results seem promising and cover the meaningful topic of providing a realistic and replicable RF propagation model on Mars, encompassing large-scale and small-scale phenomena in the presence of flat and rocky environments. The obtained parameterization of multipath propagation in terms of delays and power attenuation of the scattered replicas allows exploiting well-known channel models used in communication system simulations, like, for example, the tapped delay one.

The discussion can be widened in future work, for instance, by cropping new and larger high-resolution areas of the Martian surface and increasing the distance between transmit and receive antennas, thus experimenting longer paths, and, eventually, their height or by sweeping the working frequency. Moreover, a broadened analysis of the gathered data, also from a statistical point of view, could be helpful when selecting similar locations to test communication infrastructures to be deployed on Mars.

ACKNOWLEDGMENTS

The research activities presented in this paper fall within the field of interest of the IEEE AESS technical panel on Glue Technologies for Space Systems. Open Access Funding provided by Universita degli Studi di Trento within the CRUI-CARE Agreement. [Correction added on 27 May 2022, after first online publication: CRUI funding statement has been added.]

DATA AVAILABILITY STATEMENT

Research data are not shared.

REFERENCES

1. NASA. Mars helicopter. (Date last accessed on June 3, 2021).
2. Foust J. Independent report concludes 2033 human mars mission is not feasible. https://spacenews.com/independent-report-concludes-2033-human-mars-mission-is-not-feasible/. (Date last accessed on June 3, 2021); 2019.
3. Linck E. Evaluation of a human mission to Mars by 2033. https://www.ida.org/-/media/feature/publications/e/ev/evaluation-of-a-human-mission-to-mars-by-2033/d-10510.ashx. (Date last accessed on June 3, 2021); 2019.

4. Sacchi C, Bonafini S. From LTE-A to LTE-M: a futuristic convergence between terrestrial and Martian mobile communications. In: 2019 IEEE International Black Sea Conference on Communications and Networking (BLACKSEACOM). Sochi (RU); 2019:1-5.
5. Bonafini S, Sacchi C. Building cellular connectivity on mars: a feasibility study. In: 2020 IEEE Aerospace Conference. Big Sky (MT); 2020:1-12.
6. Fuschini F, El-Sallabi H, Degli-Esposti V, Vuokko L, Guiducci D, Vainikainen P. Analysis of multipath propagation in urban environment through multidimensional measurements and advanced ray tracing simulation. *IEEE Trans Antennas Propag*. 2008;56:848-857.
7. Hosseinzadeh S, Larijani H, Curtis K, Wixted A, Amini A. Empirical propagation performance evaluation of LoRa for indoor environment. In: 2017 IEEE 15th International Conference on Industrial Informatics (INDIN). Emden (D); 2017:26-31.
8. Mascia C. A Torino nasce il Rover Operation Control Center per ExoMars 2020. https://www.astronomia.com/2019/05/30/a-torino-nasce-il-rover-operation-control-center-per-exomars-2020/. (Date last accessed on June 3, 2021); 2019.
9. Bonafini S, Sacchi C. Evaluation of large scale propagation phenomena on the Martian surface: a 3D ray tracing approach. In: 2020 10th Advanced Satellite Multimedia Systems Conference and the 16th Signal Processing for Space Communications Workshop (ASMS/SPSC). Graz (A); 2020:1-8.
10. Bonafini S, Sacchi C. 3D ray-tracing analysis of radio propagation on mars surface. In: 2021 IEEE Aerospace Conference. Big Sky, (MT); 2021:1-9.
11. Anderson PS. Curiosity just learned that Gale crater may once have held a vast salty lake. https://earthsky.org/space/mars-curiosity-rover-ice-covered-lake-gale-crater. (Date last accessed on June 3, 2021); 2020.
12. NASA, JPL-Caltech, Arizona State University. Meridiani planum. https://mars.nasa.gov/resources/5260/meridiani-planum/. (Date last accessed on June 3, 2021); 2012.
13. NASA Science. Destination: Gusev Crater. https://science.nasa.gov/science-news/science-at-nasa/2003/30dec_gusevcrater. (Date last accessed on June 3, 2021); 2003.
14. Chukkala V, De Leon P. Simulation and analysis of the multipath environment of Mars. In: 2005 IEEE Aerospace Conference. Big Sky (MT); 2005: 1678-1683.
15. Daga A, Lovelace GR, Borah DK, De Leon PL. Terrain-based simulation of IEEE 802.11a and b physical layers on the Martian surface. *IEEE Trans Aerosp Electron Syst*. 2007;43(4):1617-1624.
16. ATDI. HTZ communications replaces ICS Telecom. https://atdi.com/ics-telecom/. (Date last accessed on June 3, 2021); 2021.
17. Greenstein LJ, Erceg V, Yeh YS, Clark MV. A new path-gain/delay-spread propagation model for digital cellular channels. *IEEE Trans Vehic Technol*. 1997;46(2):477-485.
18. Lazaridis PI, Kasampalis S, Zaharis ZD, Cosmas JP, Paunovska L, Glover IA. Longley-Rice model precision in case of multiple diffracting obstacles. In: 2015 1st URSI Atlantic Radio Science Conference (URSI AT-RASC). Gran Canaria (SP); 2015:1-1.
19. Del Re E, Pucci R, Ronga LS. IEEE802.15.4 wireless sensor network in Mars exploration scenario. In: 2009 International Workshop on Satellite and Space Communications. Siena (I); 2009:284-288.
20. Pucci R, Ronga LS, Del Re E, Boschetti D. Performance evaluation of an IEEE802.15.4 standard based wireless sensor network in mars exploration scenario. In: 2009 1st International Conference on Wireless Communication, Vehicular Technology, Information Theory and Aerospace Electronic Systems Technology. Aalborg (DK); 2009:161-165.
21. Americans Meteorological Society. Atmospheric attenuation. https://glossary.ametsoc.org/wiki/Atmospheric_attenuation; 2021.
22. NASA. Martian atmosphere and its effects on Propagation 3 .1. https://descanso.jpl.nasa.gov/propagation/mars/MarsPub_sec3.pdf; 2002.
23. NASA. Martian dust storms and their effects on propagation. https://descanso.jpl.nasa.gov/propagation/mars/MarsPub_sec5.pdf. (Date last accessed on June 3, 2021); 2002.
24. MathWorks. Math. Graphs. Programming. https://it.mathworks.com/products/matlab.html. (Date last accessed on June 3, 2021).
25. Parker T, Calef III FJ. Mars MSL Gale Merged DEM 1m v3. 2016. https://astrogeology.usgs.gov/search/map/Mars/MarsScienceLaboratory/Mosaics/MSL_Gale_DEM_Mosaic_10m. (Date last accessed on June 3, 2021).
26. Bleaney BI. *Electricity and magnetism*. Amen House, London: Oxford University Press; 1976.
27. Allen CC, Morris RV, Lindstrom DJ, Lindstrom MM, Lockwood JP. JSC Mars-1: Martian Regolith Simulant. In: Lunar and Planetary Science Conference; 1997; Houston (TX):27.
28. Morris R, Graff T, Ming D, et al. Palagonitic Mars: a basalt centric view of surface composition and aqueous alteration; 2004.
29. Cole K, Cole RH. Dispersion and absorption in dielectrics I. Alternating current characteristics. *J Chem Phys*. 1941;9:341-351.
30. Stillman D, Olhoeft G. Frequency and temperature dependence in electromagnetic properties of Martian analog minerals. *J Geophys Res Planets*. 2008; 113(E9). https://agupubs.onlinelibrary.wiley.com/doi/abs/10.1029/2007JE002977
31. Fourlis A. Reflection transmission coefficient. https://www.mathworks.com/matlabcentral/fileexchange/36531-reflection-transmission-coefficient. (Date last accessed on June 3, 2021); 2012.
32. Hosseinzadeh S. 3D ray tracing for indoor radio propagation. https://www.mathworks.com/matlabcentral/fileexchange/64695-3d-ray-tracing-for-indoor-radio-propagation. (Date last accessed on June 3, 2021); 2020.
33. Hosseinzadeh S, Larijani H, Curtis K, Wixted A, Amini A. Empirical propagation performance evaluation of LoRa for indoor environment. In: 2017 IEEE 15th International Conference on Industrial Informatics (INDIN). Emden (D); 2017:26-31.
34. McKown JW, Hamilton RL. Ray tracing as a design tool for radio networks. *IEEE Netw*. 1991;5(6):27-30.
35. Stüber GL. *Principles of Mobile Communication*. 2nd ed. USA: Kluwer Academic Publishers; 2001.
36. ITU-R. Reference standard atmospheres. https://www.itu.int/dms_pubrec/itu-r/rec/p/R-REC-P.835-6-201712-I!!PDF-E.pdf. (Date last accessed on June 3, 2021); 2017.
37. NASA. Mars facts. https://mars.nasa.gov/all-about-mars/facts/. (Date last accessed on June 3, 2021).
38. 3GPP. NR; user equipment (UE) radio transmission and reception; part 2: Range 2 Standalone. https://portal.3gpp.org/desktopmodules/Specifications/SpecificationDetails.aspx?specificationId=3284. (Date last accessed on June 3, 2021).
39. NASA. Sequence of events. https://mars.nasa.gov/MPF/mpf/realtime/mars2.html#:~:text=At%20ground%20level%20the%20Martian,_atmospheric%20pressure%20of%2014.7%20psi. (Date last accessed on June 3, 2021).
40. Clancy RT, Montmessin F, Benson J, Daerden F, Colaprete A, Wolff MJ. Mars clouds. In: Haberle RM, Clancy RT, Forget F, Smith MD, Zurek RWE, eds. *The Atmosphere and Climate of Mars*, Cambridge Planetary Science. Cambridge, UK: Cambridge University Press; 2017:76-105.
41. NASA. Martian atmospheric gaseous attenuation. https://descanso.jpl.nasa.gov/propagation/mars/MarsPub_sec4.pdf. (Date last accessed on June 3, 2021); 2009.

AUTHORS' BIOGRAPHIES

Stefano Bonafini received his B.S. in Electronics and Telecommunications Engineering and his M.S. in Information and Communications Engineering at the University of Trento, Italy. He is currently enrolled in the Ph.D. program at the ICT School of University of Trento. His studies concern interplanetary and aerospace communication systems with a particular focus on transmission techniques, channel modeling, and reconfigurable softwarized networking.

Claudio Sacchi received the "Laurea" Degree in Electronic Engineering and the Ph.D. in Space Science and Engineering at the University of Genoa (Italy) in 1992 and 2003. Since August 2002, Dr. Sacchi has been an assistant professor at the Department of Information Engineering and Computer Science (DISI) of the University of Trento (Italy). Since December 2020, he upgraded to the position of associate professor. Since 2019, he has been elected as chair of the IEEE AESS "Glue Technologies for Space Systems" technical panel. Such a panel was awarded by AESS as "Outstanding Panel of the year 2020." Claudio Sacchi is Senior Member of IEEE.

How to cite this article: Bonafini S, Sacchi C. Design of a 3D ray-tracing model based on digital elevation model for comprehension of large- and small-scale propagation phenomena over the Martian surface. *Int J Satell Commun Network*. 2022;40(6):408-427. doi: 10.1002/sat.1423